Published in final edited form as:

Ann Biomed Eng. 2015 July ; 43(7): 1502–1515. doi:10.1007/s10439-015-1252-4.

Diversity in the Strength and Structure of Unruptured Cerebral Aneurysms

Anne M. Robertson[1], **Xinjie Duan**[1], **Khaled M. Aziz**[2], **Michael R. Hill**[3], **Simon C. Watkins**[4], and **Juan R. Cebral**[5]

[1]Department of Mechanical Engineering and Materials Science, University of Pittsburgh, Pittsburgh, PA, USA

[2]Department of Neurosurgery, Allegheny General Hospital, Pittsburgh, PA, USA

[3]Institute for Computational Engineering and Sciences (ICES), University of Texas at Austin, Austin, TX, USA

[4]Center for Biological Imaging (CBI), University of Pittsburgh, Pittsburgh, PA, USA

[5]Department of Bioengineering, George Mason University, Fairfax, VA, USA

Abstract

Intracranial aneurysms are pathological enlargements of brain arteries that are believed to arise from progressive wall degeneration and remodeling. Earlier work using classical histological approaches identified variability in cerebral aneurysm mural content, ranging from layered walls with intact endothelium and aligned smooth muscle cells, to thin, hypocellular walls. Here, we take advantage of recent advances in multiphoton microscopy, to provide novel results for collagen fiber architecture in 15 human aneurysm domes without staining or fixation as well as in 12 control cerebral arteries. For all aneurysm samples, the elastic lamina was absent and the abluminal collagen fibers had similar diameters to control arteries. In contrast, the collagen fibers on the luminal side showed great variability in both diameter and architecture ranging from dense fiber layers to sparse fiber constructs suggestive of ineffective remodeling efforts. The mechanical integrity of eight aneurysm samples was assessed using uniaxial experiments, revealing two sub-classes (i) vulnerable unruptured aneurysms (low failure stress and failure pressure), and (ii) strong unruptured aneurysms (high failure stress and failure pressure). These results suggest a need to refine the end-point of risk assessment studies that currently do not distinguish risk levels among unruptured aneurysms. We propose that a measure of wall integrity that identifies this vulnerable wall subpopulation will be useful for interpreting future biological and structural data.

Keywords

Soft tissue; Rupture risk; Structural integrity; Collagen; Failure; Multiphoton; Remodeling

Address correspondence to Anne M. Robertson, Department of Mechanical Engineering and Materials Science, University of Pittsburgh, Pittsburgh, PA, USA. Electronic mail: rbertson@pitt.edu.

Associate Editor Gerhard A. Holzapfel oversaw the review of this article.

CONFLICT OF INTEREST

None.

INTRODUCTION

Intracranial aneurysms (IAs) are pathological dilatations of the cerebral arteries that have serious consequences when they rupture.[31] Cadaveric studies have demonstrated a large incidence in the general population, between 5 and 8%.[22,37] Although the rupture rate of incidental aneurysms is very low (estimated at 0.3–3% per year),[13,20,21,35] subarachnoid hemorrhage secondary to aneurysm rupture carries large morbidity and mortality rates (45% fatality rate, and 64% long term disability rate).[16,26] However, surgical and endovascular interventions have associated risks. In fact, the hemorrhagic and ischemic risks associated with aneurysm interventions can exceed the natural risk of rupture (the estimated combined morbid-mortality rate is 10–14% during the first month).[2,35] Therefore, clinicians and patients often face the important question of whether to intervene or conservatively follow the aneurysm. Anatomical information (size, location, and presence of blebs or blister morphology), patient's age, and clinical status (prior rupture, family history, and smoking) provide some help in predicting the natural history of brain aneurysms.[18] Currently, aneurysm size is the main anatomical measure commonly used to assess rupture risk. However, aneurysms below the identified size threshold (7 mm) still account for a substantial number of ruptures.[18,36] Improving current aneurysm assessment and the clinical decision making process requires an understanding of the underlying mechanisms governing the natural history of cerebral aneurysms.

It is generally accepted that the evolution of IAs is driven by flow-induced progressive degradation of the wall.[6,9,12] For example, based on histological analysis of resected human aneurysm tissue, Frösen *et al*. suggested that aberrant aneurysmal flow conditions likely cause endothelial dysfunction which induces accumulation of cytotoxic and pro-inflammatory substances in the wall as well as thrombus formation, that in turn result in loss of mural cells and wall degeneration.[9] However, the detailed mechanisms and interactions between the many factors involved in the development, enlargement, and rupture of cerebral aneurysms remain poorly understood.[6]

Most previous studies have focused on connecting clinical, geometric, and hemodynamic information to the aneurysm rupture state in order to identify conditions that could be used to assess the risk of rupture.[6] While these investigations have produced valuable information and have guided the clinical decision making process, they have not significantly improved our knowledge of the underlying mechanisms governing the natural history of IAs. Therefore, in parallel to those studies, we believe it is important to identify other end points in *ex vivo* studies (such as aneurysm failure characteristics) that could be used to assess the vulnerability of cerebral aneurysms and connect them to patient status, anatomical characteristics, flow conditions, and wall mechanical environment.

The aneurysm wall contains a heterogeneous population of cells types that are responsible for the maintenance and repair of the underlying collagen matrix. The state of this matrix determines the structural integrity of the aneurysm. Earlier work by Frösen *et al*. evaluated the cell content and extracellular matrix of human aneurysm domes resected during surgery and proposed a histological categorization of four aneurysm wall types.[8] While one

subcategory was always associated with rupture, the other categories were associated with both unruptured and ruptured aneurysms.

The purpose of the current work is to assess the diversity of wall strength and extracellular matrix in even unruptured human IAs. We take advantage of recent advances in multiphoton microscopy to provide novel results for the architecture of collagen fibers in the intact aneurysm samples without staining or fixation.[11]

MATERIALS AND METHODS

Aneurysm Tissue Retrieval and Handling

Aneurysm domes were harvested following surgical clipping in consented patients being treated for unruptured aneurysms at the Allegheny General Hospital. The harvested tissue was placed in a vial of 0.9% (w/v) saline solution, stored in an insulated cooler and transported to the University of Pittsburgh. Mechanical testing was performed on aneurysm samples within 48 h. The protocols for patient consent, handling of patient data, tissue harvest, and analysis were approved by the institutional review boards (IRB) at both the Allegheny General Hospital and the University of Pittsburgh. While 46 patients were consented for the study, based on clinical decisions at the time of treatment, tissue was harvested from 15 patients.

Human basilar arteries ($n = 6$) and internal carotid arteries ($n = 6$) were obtained from the circles of Willis of human cadavers from patients that died from causes unrelated to cerebral aneurysms (Brain Bank of the University of Pittsburgh). The Circles of Willis were harvested from these cadavers during autopsy, snap frozen and stored at −80 °C. Prior to testing, the tissue was thawed at room temperature and circumferential sections removed.

Patient Clinical Data

Clinical data was collected for each patient including gender, age, and family history of IAs. Lifestyle and health information including cigarette smoking, hypertension, diabetes mellitus and treatment with statins were obtained. Patients were considered positive for hypertension if they were currently being treated for hypertension or if they were previously diagnosed with hypertension but declined treatment. Smoking status was reported with respect to packs of cigarettes per week. Patients were categorized as non-smokers if they had never smoked cigarettes or had not smoked within the last 5 years. Patients who currently smoked or who had quit within the last 5 years were categorized as smokers. Notation was made of patients who used smokeless tobacco (snuff). Assessment of number of aneurysms, SAH status and aneurysm location was made from CT. In cases of multiple aneurysms, choice of aneurysm for tissue harvest was based on patient need. The control arteries were obtained for eight males and four females with an average age of 80.8 ± 10.6.

Morphology Assessment

Vascular models of the aneurysm and connected arteries were constructed from 3D rotational angiography images. Unstructured volumetric grids composed of tetrahedral elements were generated to fill the interior of the vascular models. The mesh resolution was

approximately 0.2 mm. The aneurysm neck was delineated by connecting points interactively selected on the vascular reconstructions following paths of minimal geodesic distance. The aneurysm orifice, defined by the neck contour, was triangulated and used to label mesh points on each side as “aneurysm” or “parent artery”. The following geometric quantities were then calculated (see Cebral *et al*.[5] for further details of these definitions): (1) aneurysm volume: computed by adding the volume of all tetrahedral elements within the aneurysm region; (2) aneurysm surface area: computed by summing the area of all triangles of the surface mesh within the aneurysm region; (3) equivalent sac diameter: diameter of a sphere of volume equal to the aneurysm volume; (4) maximum aneurysm size: computed as the maximum Euclidean distance between any two points in the aneurysm region; (5) aneurysm depth (sometimes referred to as height): computed as the length of the maximal path from any aneurysm point to the orifice surface; (6) neck area: computed by adding the areas of all the triangles of the orifice surface; (7) neck maximum size: computed as the maximum Euclidean distance between any two points on the orifice surface; and (8) aspect ratio: defined as the ratio between the aneurysm depth over the maximum aneurysm neck size.

Mechanical Testing Protocol

Aneurysm and artery wall samples were tested in a custom designed uniaxial loading system compatible with an Olympus FV1000 MPE multiphoton microscope (Tokyo, Japan).[11,23] Using this UA-MPM system, it is possible to simultaneously perform mechanical testing and structural imaging under MPM (“Multiphoton Imaging and Post-processing” section). Rectangular strips of the aneurysm were obtained in the meridional direction. Circumferential strips of artery were cut from cerebral arteries from the human circles of Willis. Unloaded wall thickness was measured at five positions using micro-calipers and averaged. The test samples were gripped by mechanical clamps[11] and placed in a bath of 0.9% (w/v) saline at room temperature in the UA-MPM system. Fine-grade sandpaper was adhered to tissue-contacting surfaces on the UA-MPM device to avoid the need for adhesives. Eight of the 15 samples met the minimum size of 4 mm × 5 mm necessary for mechanical testing.

Specimens were subjected to uniaxial extension at a speed of 20 μm/s along the meridional direction for aneurysm and circumferential direction for artery. Displacement was controlled by a linear actuator (ANT-25LA, Aerotech, PA), and force was recorded with a 5 lb load cell (MDB-5, Transducer Techniques, Rio Nedo Temacula, CA). Force vs. displacement curves were obtained after five cycles of preconditioning to 0.3 N and used to calculate Cauchy stress as a function of stretch. Zero strain was defined as the configuration of the tissue under 0.005 N load. Current area was calculated from the unloaded cross sectional area and longitudinal strain assuming an isochoric deformation. For purposes of quantitative comparison between samples, a simple exponential model for the strain energy function (per unit volume) was fit to the mechanical data

$$W=\frac{C_1}{2C_2}\left(e^{C_2(I_1-3)^2}-1\right) \quad (1)$$

The loading curves were broken into four regions, a nearly linear toe region (low stress response), a transition region, a nearly linear post transition-pre-failure region (high stress response), and a sub-failure region. Low stress stiffness was defined as the slope of a linear fit for the toe region, and high stress stiffness as the slope of a linear fit for the high stress region (in the post-transition and pre-failure region). The transition stretch was defined as that corresponding to the point of intersection of the two fitted lines.

Multiphoton Imaging and Post-processing

Collagen and elastin content in the samples were assessed using multiphoton microscopy (MPM). An Olympus FV1000 MPE (Tokyo, Japan) equipped with a Spectra-Physics DeepSee Mai Tai Ti–Sapphire laser (Newport, Mountain View, CA) with an 1.12NA 25× MPE water immersion objective was used for all samples. The excitation wavelength was 870 nm. The second harmonic generation (SHG) signals from collagen were collected using non-descanned, backscatter epi detectors and 400 nm Chroma emission filters with a 50 spectral bin (Brattleboro, VT). The dwell time was 10 μs/pixel at a scan pixel count of 1024 × 1024. An in plane resolution of 0.12 μm was achieved with this system.

The en face images were obtained for fresh samples loaded in the UA-MPM system. Samples were imaged from both luminal and abluminal sides (termed luminal and abluminal images, respectively), with stacks commencing from the layer furthest from the lens and moving upward in 2 μm intervals. Fiber diameters were measured (Image J) at 15 randomized locations in superposed stacks (Imaris, Bitplane) of MPM images. In cases where fibers were banded, diameters of individual fibers were used.

Images were obtained from some fixed samples that were sectioned in a cross sectional cut in order to assess the collagen architecture across the wall thickness. These samples were fixed in 2% paraformaldehyde in PBS at 4 °C for 4 h, and slowly frozen in liquid nitrogen. Eight micron thick sections were obtained by slicing the sample with a cryostat (HM 505E, Microm). Slides were kept at 20 °C until ready for use.

Statistical Analysis

Linear regression analysis was carried out to test for possible correlations between wall thickness and other geometric parameters. The slope of the linear regression was considered significantly different from zero if the corresponding p values were below 0.05. The non-parametric Wilcoxon test was used to test whether the mean values of material properties of different groups of tissue samples (e.g., aneurysms against control arteries) were statistically different. Differences were considered statistically significant if the p values were less than 0.05 (95% confidence). All statistical analysis was performed using the Python SciPy package.

RESULTS

Study Population

Fifteen unruptured IAs were included in this study of which ten were symptomatic, Table 1. No patients had signs of subarachnoid hemorrhage. Eight of the patients were female and the

mean and median patient ages were 56 and 57 respectively. Notably, the patient population included a 27 year old, whose aneurysm was found incidentally and had no other identifiable medical conditions and no reports of drug use. Nine of the patients had multiple aneurysms and five had a family history of cerebral aneurysms. Of the resected aneurysms, 8 (53%) were from the middle cerebral artery (MCA), 4 (27%) were from the internal carotid artery (ICA), 2 (13%) were from the anterior cerebral artery ACA and 1 (7%) was from the anterior communicating artery (AcomA).

Morphology of the Aneurysm Sac and Dome

The equivalent diameters of the aneurysms ranged from 4.4 to 11.1 mm, Table 2. No correlation was found between wall thickness, which ranged from 130 to 450 μm and any other geometric parameters of the sac in Table 2. In particular, the wall thickness was not linearly related to the aneurysm equivalent diameter.

Subfailure Properties

The loading curves for the uniaxial loading tests to failure for eight aneurysm samples are shown in Fig. 1 with a magnified insert to show the low stress region. These curves are shown relative to the corresponding results for the control cerebral arteries in Fig. 2. The loading curves for both the control arteries and aneurysm tissue are qualitatively exponential in shape, with the exception of Sample CA-11, Fig. 1. This is consistent with the lower R^2 value for the fit of the exponential hyperelastic strain energy function to the data for CA-11, Table 3.

The toe region for the aneurysm tissue is noticeably shortened relative to the control arteries with a stiffer response than that seen in the control arteries, Fig. 2, which is consistent with the lack of internal elastic lamina in the aneurysm tissue (discussed below). The difference in low stress stiffness between the aneurysm and all control arteries is statistically significant with a p value of 0.021, whereas the high stress stiffness did not reach statistical significance ($p = 0.06$). There was no statistical difference between the stiffness of the basilar and carotid arteries ($p = 0.784$ for low strain stiffness and $p = 0.632$ for high strain stiffness).

Failure Properties

Failure stress values for the aneurysm tissue fell into distinct low and high failure stress categories, Fig. 2. The failure stress (Cauchy) for the two low strength walls was 0.63 and 0.73 MPa, with an average of 0.68 ± 0.08 MPa, Table 3. These two weaker samples (CA-11, CA-15) were qualitatively quite different from each other, suggesting distinct failure modes. CA-15 had the smallest toe region of any of the samples, while the response of CA-11 was more linear than all other aneurysm samples, and comparatively stiffer at low stress and softer at high stress. Samples CA-11 and CA-15 displayed the extremes of high stress stiffness with values of 3.42 and 25.1 MPa, respectively. In contrast, the high strength samples had a mean high stress stiffness of 11.8 ± 4.6 MPa.

The high strength aneurysms (CA-1, CA-12, CA-25, CA-26, CA-39, CA-46) displayed a more uniform response. The low stress stiffness had a mean of 0.46 ± 0.28 MPa. The Cauchy ultimate stress of the high strength aneurysms ranged from 1.2 to 2.2 MPa with an

average of 1.6 ± 0.36 MPa. The strength of even the high strength aneurysms was significantly lower ($p = 0.001$) than that of the basilar arteries that ranged from 2.7 to 3.3 MPa with an average of 3.0 ± 0.26 MPa and those of the internal carotid arteries from 2.6 to 3.5 MPa with an average of 3.0 ± 0.29 MPa. Differences between the ultimate stress of basilar and carotid arteries were not statistically significant ($p = 0.908$).

While the stress provides information about the material properties, failure tension, which is equal to the product of the failure stress (engineering) and unloaded thickness, provides a measure of the ability of the wall to withstand loading. For example, while the failure stress of CA-25 and CA-26 are quite similar, the thickness of CA-26 is nearly twice that of CA-25, resulting in a much larger ability to bear load. Namely, sample CA-26 has a failure tension of 580 kg/s^2, compared with 280 kg/s^2 for CA-25. This increased failure tension is necessary, given the increased intramural loading in CA-26 due to its larger equivalent diameter, Table 2. Following prior work,[3,33] we use a simple equilibrium equation for spherical membranes loaded under uniform pressure (Laplace's Law) and estimate the transmural pressure under which each aneurysm would fail ΔP_f,

$$\Delta P_f = 4\sigma \frac{t_0}{D}\left(\frac{D}{d}\right)^3 \quad (2)$$

where σ is the ultimate Cauchy stress, D is the effective (unloaded diameter), t_0 is the wall thickness (unloaded) and d is the loaded diameter. If we conservatively estimate the failure radius as 1.05 times the unloaded radius, then domes of CA-11, CA-15 would fail with ΔP_f of 454 and 264 mmHg, respectively, whereas the estimated failure pressures of the higher strength domes range from 945 to 3300 mmHg. During weight training, arterial pressures can rise well above 200 mmHg.[19] For example, in a study of five healthy males performing leg press repetitions, the group mean for peak pressures was 320/250 mmHg and rose as high as 480/350 mmHg in one individual.[19] If we consider 180 mmHg as a design load, then the factor of safety for CA-15 and CA-11 are 1.5 and 2.5, respectively, whereas the values for the stronger group range from 5.25 to 18.4. Motivated by the reported pressures during weight training, we might select a design load of 300 mmHg. In this case, the factor of safety would drop to 1.5 for CA-11 and CA-15 would fail.

Wall Structure

The passive load bearing components in healthy arteries are elastin and collagen, (e.g., Ref. 25). In cerebral vessels, the elastin is nearly confined to the internal elastic lamina, shown in green in Fig. 3a. Medial collagen fibers are wavy in the unloaded vessel, Figs. 3b and 5. The adventitial collagen fibers display a larger range of fiber angles and fiber diameters than the medial collagen fibers, Fig. 3c. In contrast, no elastin is visible in the MPM images of the aneurysm wall (not shown), consistent with prior reports of the aneurysm wall.[1,31] When viewed from the luminal side, there is a great variability in the fiber architecture and diameter between aneurysm samples, Fig. 3. In some samples, the collagen fibers are densely packed, for example CA-12 in Fig. 3 and CA-26 in Fig. 4a. In others, there is an abnormal sparse structure, for example CA-21. When viewed in a cross-sectional slice under MPM, the densely packed fibers of CA-26 can be seen to form a layered collagen structure, Fig. 4b. The average wall thickness for sample CA-26 is 0.45 μm, substantially thicker than

the average of 0.277 μm found for basilar arteries, Table 2. The average diameter of the collagen fibers on the luminal side is 0.99 μm and is statistically different from the average of 1.325 μm in the media of the basilar artery ($p = 0.001$), suggesting a change in the fiber maintenance and/or creation process, Fig. 5. In contrast, the average diameter of the collagen fibers from the abluminal side of the aneurysm wall is not statistically different from that of the basilar arteries ($p = 0.42$).

Recruitment of Abluminal Collagen

In order to better understand the role of adventitial collagen during loading, collagen fibers were imaged from the abluminal side of a representative sample during uniaxial loading with the UA-MPM system, Fig. 6. In the unloaded tissue, the abluminal collagen architecture was relatively disorganized with a wide range of fiber orientations. With increasing loads, fibers can be seen to be recruited to load bearing *via* two mechanisms—fiber straightening and fiber reorientation, consistent with recruitment mechanisms in healthy control arteries.[11] The fibers are nearly aligned by a stretch of 1.3, in line with the marked increase stiffness. At stretches lower than 1.2, the wall is approximately 30 times more compliant than the response in the high stress region.

DISCUSSION

In this work, we have demonstrated that even the unruptured population of cerebral aneurysms displays a diversity of mechanical properties and collagen architecture. Moreover, the current results suggest the existence of distinct sub-populations in the group of unruptured aneurysms: (1) more fragile aneurysms with failure properties similar to those of ruptured aneurysms, and (2) those well suited for load bearing under physiological conditions. The first group can be considered more vulnerable in that the estimated pressure loading for failure was closer to physiological attainable levels with a safety factor for loading to 180 mmHg of 1.5 and 2.5. In contrast, the second group could be considered robust at the time of harvest. Even though they were found to be statistically weaker than cerebral arteries, they were strong relative to expected physiological loads with safety factors of 5.26 and higher.

The possibility that rupture of a vulnerable aneurysm can be triggered by mechanical loads is supported by the fact that aneurysm rupture is often associated with strenuous physical activity including weight training.[10,28] For example, in a study population of 445 patients, 42.8% of the ruptures aneurysms were associated with physical or emotional stress (e.g., Ref. 28). This possibility is also consistent with the similarity between the failure strength of the weaker group and reported strength of ruptured aneurysms.

A large spread in mechanical strength of unruptured aneurysms was also reported by Scott *et al*.[30] They evaluated the failure pressure for two unruptured human aneurysms (obtained at autopsy) by pressurizing the domes with saline solution. A 5 mm aneurysm ruptured at 325 mmHg whereas a 6 mm aneurysm remained unruptured even during repeated loads up to 550 mmHg. Interestingly, the failure pressure of the weaker of these aneurysms lies between the two values of the weaker group in our study, and the 6 mm aneurysm was at least as strong as the weaker members of the robust group. The average values for the peak systolic

and diastolic pressure was reported to be 320/250 mmHg during weight training, suggesting this first aneurysm was vulnerable to rupture under extreme physiologically attainable conditions.[30]

Though the failure stresses for the walls of the vulnerable group in our study were similar, the loading curves were qualitatively different, suggesting different pathologies. The high strength aneurysms displayed a greater uniformity in mechanical response with smaller variation of failure stresses, high stress stiffness and toe region. Sample CA-11 was resected from the only diabetic patient. This patient was asymptomatic and the aneurysm walls were of normal thickness, relative to the control arteries. The loading curve for this sample was qualitatively different from all others with a relatively poor fit to the exponential constitutive model. In contrast, sample CA-15 had one of the thinnest walls and a greatly shortened toe region relative to the other samples. Further, the abluminal collagen fibers of CA-15 demonstrated a morphology that was markedly different from all other samples.

A healthy cerebral artery is composed of three distinct wall layers. Moving from the lumen to the abluminal side, these layers are the intima which is separated from the medial layer by an internal elastic lamina (IEL), followed by the adventitia, Fig. 3a. Collagen fiber diameters, measured from MPM images of the control arteries demonstrated a statistical difference in the collagen fiber diameter in the adventitial and medial layers with larger fiber diameters being located in the adventitial layer, consistent with the differences in collagen types found in these layers. For example, collagen I fibers are nearly entirely confined to the adventitial layer of cerebral arteries, with small amounts in the basement membrane of the endothelial cells.[1] In contrast, collagen type III is largely restricted to the medial layer. With the exception of one sample (CA-9), distinct collagen diameters were also identified from the luminal and abluminal views of the aneurysm tissue. In all other samples, the collagen layer on the luminal side was significantly different between aneurysm and control, suggesting the normal turnover of collagen fibers on the luminal (media originating) side is substantially impacted relative to the control artery. This is consistent with the large range of abnormal collagen architecture seen in this layer. In contrast, the diameter of the abluminal collagen fibers were similar to those found in the adventitia of the control arteries, suggesting an adventitial origin of this tissue. The findings for collagen fiber diameter in CA-9 appear to be of entirely adventitial type and suggest a different mechanism of remodeling. Differences in load bearing capacity in the medial layer across samples is certainly a contributing factor for the diversity in the adventitial remodeling and warrants further investigation (e.g., Ref. 29).

Consistent with other reports, there was no IEL seen in any of the aneurysm samples. The loss of the IEL has structural implications as seen in the reduced toe region of the aneurysm tissue relative to the control cerebral arteries. The IEL also acts as a barrier or impediment to cellular movement and other transport between the endothelium and medial layers. The absence of this barrier might be expected to have a substantial impact on the cellular activities related to wall maintenance.

Recently, it has been reported that ruptured aneurysms have diminished stiffness relative to unruptured aneurysms, when separated by gender.[7] Further, it has been suggested that the

larger deformations arising from the diminished wall stiffness could possibly be used to identify aneurysms at risk for rupture, when improved clinical imaging modalities become available.[27] This conjecture addresses the important issue of identifying a clinically accessible metric for identifying at risk aneurysms. The range of strains considered in those uniaxial loading studies was less than 15%, and corresponds to the magnified region in Fig. 1. It can be seen that the two vulnerable aneurysms in the current study had the highest low stress stiffness, in contrast to this earlier study. The present results suggest that aneurysms that are stiffer at low stress are not stronger. In fact, the more robust aneurysm walls displayed values of low stress stiffness that were closer to control arteries wall. Namely both were softer at low loads than the vulnerable aneurysms studied in this work. Further investigations are warranted on this subject.

Uniaxial loading was used to assess the failure properties of the cerebral aneurysm tissue. While uniaxial testing is commonly used for failure testing, it should be recognized that *in vivo* loading of cerebral aneurysm walls is closer to equibiaxial than uniaxial. As shown in Fig. 6, under uniaxial loading, collagen fibers experienced large reorientation up until stretches of approximately 1.25. Under equibiaxial loading, reorientation of this kind would not be seen. Therefore, the low stress regions shown in Fig. 1 provide information about the ability of the fibers to reorient and uncrimp rather than providing information about collagen load bearing relevant to physiological biaxial loading conditions. We caution against using material properties obtained from low stress, uniaxial loading to model biaxial aneurysm deformations. The aneurysm wall is an anisotropic material, and therefore, the anisotropic response cannot be determined from uniaxial experiments, in the absence of other information about the fiber structure. We emphasize that material properties were obtained in this work for a relatively simple phenomenological model for the purpose of characterizing the mechanical response. The use of a structurally motivated model that incorporates fiber recruitment and fiber orientation such as was introduced in Hill *et al.*[11] is the subject of an ongoing investigation.

It should be noted that the control cerebral arteries used in this study were stored at −80 °C prior to testing. Stemper *et al.* reported that the uniaxial mechanical properties, including high-strain stiffness and ultimate stresses of porcine aortas were not significantly different between fresh samples and those stored at −80 °C for 3 months.[34]

For a given hemodynamic waveform, the nature of the local mechanical loads on the aneurysm wall (both surface shear and intramural stresses) are largely a function of the geometry of the parent vasculature and aneurysm sac. Intramural loads that vary too greatly from physiological levels can negatively impact the cellular health. It is believed that some, as yet unidentified aspect, of the intra-saccular flow leads to a degeneration of the endothelium, that can in turn negatively influence the wall cellular content and ultimately interfere with the normal process of collagen renewal and maintenance (e.g., Refs. 9,14,17, and 32). Prior efforts to identify clinically useful methods for risk stratification, have therefore focused on identifying correlations between rupture status and clinically accessible quantities such as sac geometry and intra-saccular hemodynamics, Fig. 7. Work is ongoing to identify a clinically useful metric that goes beyond the current use of aneurysm size. More recently, efforts have been made to correlate intramural cell content and rupture status.[8]

Frösen *et al.* have clearly demonstrated the great variability in cell content in aneurysm walls. The intramural content of even an unruptured aneurysm was found to vary from an endothelialized wall with linearly organized smooth muscle cells (SMCs) to a hypocellular wall.[8,9]

The current findings complement these earlier studies, demonstrating a variability in collagen content and mechanical properties within even the unruptured population that is consisted with this range of intramural cell content. Namely, given the large range of cell content in unruptured walls, we would expect the collagen fabric that is maintained by these cells should also vary, as should the mechanical properties which are dependent on the collagen fabric.

To date, a definitive rupture index using hemodynamic, geometric or biological markers has not been identified.[4,9,15,24] The existence of a subpopulation of unruptured aneurysms with failure properties similar to those of ruptured aneurysms underlines the challenge in using rupture status as an endpoint to interpret data. Namely, if the objective is to predict whether an aneurysm is vulnerable to rupture, then categorizing a vulnerable unruptured aneurysm as safe can confound the interpretation of the data, since this aneurysm may soon rupture under suitable triggers. In cases where it is possible to obtain resected aneurysm tissue, we can overcome this limitation in classification by looking for correlations with an index of wall integrity rather than rupture status, Fig. 7. Such an index would account for the combined effect of material properties (e.g., failure stress), geometry (e.g., wall thickness, shape, and diameter), and expected loads through, for example, a factor of safety. While such an integrity index is not yet useful in the clinic, we believe it will be valuable for future studies of wall biology and provide a more solid framework for understanding the mechanisms responsible for aneurysm wall degradation. Insights gained from studies using an index of wall integrity may enable more effective use of clinically available data such as aneurysm hemodynamics. Ultimately, an improved understanding of the mechanisms responsible for the progressive degeneration or stabilization of cerebral aneurysms will be useful for development of improved treatment strategies.

CONCLUSIONS

This work is the first to combine MPM imaging with mechanical testing for studying the pathology of human cerebral aneurysms. Using this approach, we found substantial variability in collagen architecture and mechanical response even within walls of unruptured aneurysms. This variability is consistent with earlier studies using classical histological approaches that found a large variability in mural content, even within unruptured human aneurysms domes.[8]

The collagen architecture on the luminal side of the aneurysms was generally quite different from the healthy artery and showed a great variability between samples. Some samples displayed a dense fiber network, likely produced through remodeling mechanisms. Others had a sparse, inhomogeneous fiber architecture suggestive of impaired remodeling. Fibers from the luminal side were nearly always thinner compared with medial fibers in normal

arteries. In contrast, the abluminal side was more similar to the adventitia of healthy arteries with respect to fiber diameter and orientation.

Even unruptured aneurysms displayed a wide range of mechanical behaviors. Two sub-categories were identified: (i) vulnerable aneurysms with lower failure stress and lower estimated failure pressure, and (ii) more robust aneurysms with higher failure stress and higher estimated failure pressure. Although the stronger aneurysm walls were weaker than control arteries, they were strong relative to estimated physiological loads with a safety factor of 5.2 and higher, suggesting an effective remodeling process. In contrast, the failure stress of the vulnerable aneurysms was similar to values reported for ruptured aneurysms and had factors of safety of 2.5 and less. Such a sub-categorization of unruptured aneurysms is therefore an important consideration when using rupture as an end-point of risk assessment studies.

This work suggests a structural integrity index will be useful for interpreting biological and hemodynamic data in future investigations of the mechanisms responsible for the progressive degeneration of the wall of IAs.

Acknowledgments

This work was supported, in part, by a grant from the National Institute of Neurological Disorders and Stroke of the National Institute of Health (1R21NS080031-01A1). We also wish to acknowledge Joshua Selling, a talented undergraduate student at the University of Pittsburgh, for his development and implementation of a meticulous protocol for fiber diameter measurements. The authors wish to thank the Alzheimers Disease Research Center (ADRC) of the University of Pittsburgh and Dr. Julia K. Kofler, Director of the Neuropathology Core of the ADRC for providing the cadaveric human cerebral vessels that were used in this study.

References

1. Austin G, Fisher S, Dickson D, Anderson D, Richardson S. The significance of the extracellular matrix in intracranial aneurysms. Ann Clin Lab Sci. 1993; 23(2):97–105. [PubMed: 7681275]
2. Broderick JP, Brown RD, Sauerbeck L, Hornung R, Huston J, Woo D, Anderson C, Rouleau G, Kleindorfer D, Flaherty ML, Meissner I, Foroud T, Moomaw ECJ, Connolly ES. Greater rupture risk for familial as compared to sporadic unruptured intracranial aneurysms. Stroke. 2009; 40:1952–1957. [PubMed: 19228834]
3. Canham PB, Ferguson GG. A mathematical model for the mechanics of saccular aneurysms. J Neurosurg. 1985; 17:291–295.
4. Cebral JR, Meng H. Counterpoint: realizing the clinical utility of computational fluid dynamics—closing the gap. AJNR Am J Neuroradiol. 2012; 33(3):396–398. [PubMed: 22282452]
5. Cebral JR, Mut F, Weir J, Putman C. Quantitative characterization of the hemodynamic environment in ruptured and unruptured brain aneurysms. AJNR Am J Neuroradiol. 2011; 32(1): 145–151. [PubMed: 21127144]
6. Cebral JR, Raschi M. Suggested connections between risk factors of intracranial aneurysms: a review. Ann Biomed Eng. 2013; 41:1366–1383. [PubMed: 23242844]
7. Costalat V, Sanchez M, Ambard D, Thines L, Lonjon N, Nicoud F, Brunel H, Lejeune JP, Dufour H, Bouillot P, Lhaldky JP, Kouri K, Segnarbieux F, Maurage CA, Lobotesis K, Villa-Uriol MC, Zhang C, Frangi AF, Mercier G, Bonafé A, Sarry L, Jourdan F. Biomechanical wall properties of human intracranial aneurysms resected following surgical clipping (IRRAs Project). J Biomech. 2011; 44(15):2685–2691. [PubMed: 21924427]
8. Frösen J, Piippo A, Paetau A, Kangasniemi M, Niemelä M, Hernesniemi J, Jääskeläinen J. Remodeling of saccular cerebral artery aneurysm wall is associated with rupture: histological

analysis of 24 unruptured and 42 ruptured cases. Stroke. 2004; 35(10):2287–2293. [PubMed: 15322297]

9. Frösen J, Tulamo R, Paetau A, Laaksamo E, Korja M, Laakso A, Niemelä M, Hernesniemi J. Saccular intracranial aneurysm: pathology and mechanisms. Acta Neuropathol. 2012; 123(6):773–786. [PubMed: 22249619]
10. Haykowsky MJ, Findlay JM, Ignaszewski AP. Aneurysmal subarachnoid hemorrhage associated with weight training: three case reports. Clin J Sport Med. 1996; 6(1):52–55. [PubMed: 8925367]
11. Hill M, Duan X, Gibson G, Watkins S, Robertson A. A theoretical and non-destructive experimental approach for direct inclusion of measured collagen orientation and recruitment into mechanical models of the artery wall. J Biomech. 2012; 45(5):762–771. [PubMed: 22305290]
12. Humphrey JD, Canham PB. Structure, mechanical properties, and mechanics of intracranial saccular aneurysms. J Elasticity. 2000; 61:49–81.
13. Juvela S, Porras M, Poussa K. Natural history of unruptured intracranial aneurysms: probability of and risk factors for aneurysm rupture. J Neurosurg. 2008; 108(5):1052–1060. [PubMed: 18447733]
14. Kadirvel R, Ding YH, Dai D, Zakaria H, Robertson A, Danielson M, Lewis D, Cloft H, Kallmes D. The influence of hemodynamic forces on biomarkers in the walls of elastase-induced aneurysms in rabbits. Neuroradi-ology. 2007; 49(12):1041–1053.
15. Kallmes DF. Point: CFD—computational fluid dynamics or confounding factor dissemination. AJNR Am J Neuroradiol. 2012; 33(3):395–396. [PubMed: 22268081]
16. Kelly PJ, Stein J, Shafqat S, Eskey C, Doherty D, Chang Y, Kurina A, Furie KL. Functional recovery after rehabilitation for cerebellar stroke. Stroke. 2001; 32(2):530–534. [PubMed: 11157193]
17. Krings T, Mandell DM, Kiehl TR, Geibprasert S, Tymianski M, Alvarez H, TerBrugge KG, Hans FJ. Intracranial aneurysms: from vessel wall pathology to therapeutic approach. Nat Rev Neurol. 2011; 7(10):547–559. [PubMed: 21931350]
18. Lall R, Eddleman C, Bendok B, Batjer H. Unruptured intracranial aneurysms and the assessment of rupture risk based on anatomical and morphological factors: sifting through the sands of data. Neurosurg Focus. 2009; 26(5):E2. [PubMed: 19408998]
19. MacDougall JD, Tuxen D, Sale DG, Moroz JR, Sutton JR. Arterial blood pressure response to heavy resistance exercise. J Appl Physiol. 1985; 58:785–790. [PubMed: 3980383]
20. Morita A, Fujiwara S, Hashi K, Ohtsu H, Kirino T. Risk of rupture associated with intact cerebral aneurysms in the Japanese population: a systematic review of the literature from Japan. J Neurosurg. 2005; 102(4):601–606. [PubMed: 15871500]
21. Morita A, Kimura T, Shojima M, Sameshima T, Nishihara T. Unruptured intracranial aneurysms: current perspectives on the origin and natural course, and quest for standards in the management strategy. Neurol Med Chir. 2010; 50(9):777–787.
22. Rinkel G, Djibuti M, Agra A, Gijn JV. Prevalence and risk of rupture of intracranial aneurysms: a systematic review. Stroke. 1998; 29:251–256. [PubMed: 9445359]
23. Robertson, AM.; Hill, MR.; Li, D. Structurally motivated damage models for arterial walls—theory and application. In: Ambrosi, D.; Quarteroni, A.; Rozza, G., editors. Modelling of Physiological Flows, Modeling, Simulation and Applications. Vol. 5. New York: Springer; 2011.
24. Robertson AM, Watton PN. Computational fluid dynamics in aneurysm research: critical reflections, future directions. AJNR Am J Neuroradiol. 2012; 33(6):992–995. [PubMed: 22653325]
25. Robertson, AM.; Watton, PN. Mechanobiology of the arterial wall, chap 8. In: Becker, S.; Kuznetsov, A., editors. Transport in Biological Media. New York: Elsevier; 2013. p. 275-347.
26. Ropper AH, Zervas NT. Outcome 1 year after SAH from cerebral aneurysm. Management morbidity, mortality, and functional status in 112 consecutive good-risk patients. J Neurosurg. 1984; 60:909–915. [PubMed: 6716158]
27. Sanchez M, Ambard D, Costalat V, Mendez S, Jourdan F, Nicoud F. Biomechanical assessment of the individual risk of rupture of cerebral aneurysms: a proof of concept. Ann Biomed Eng. 2013; 41:28–40. [PubMed: 22864824]

28. Schievink WI, Karemaker JM, Hageman LM, van der Werf DJ. Circumstances surrounding aneurysmal subarachnoid hemorrhage. Surg Neurol. 1989; 32(4):266–272. [PubMed: 2675363]
29. Schmid H, Watton PN, Maurer MM, Wimmer J, Winkler P, Wang YK, Röhrle O, Itskov M. Impact of transmural heterogeneities on arterial adaptation: application to aneurysm formation. Biomech Model Mechanobiol. 2010; 9:295–315. [PubMed: 19943177]
30. Scott S, Ferguson GG, Roach MR. Comparison of the elastic properties of human intracranial arteries and aneurysms. Can J Physiol Pharmacol. 1972; 50:328–332.10.1139/y72-049 [PubMed: 5038350]
31. Stehbens, WE. Pathology of the Cerebral Blood Vessels. St. Louis: C.V. Mosby Co.; 1972.
32. Stehbens WE. Etiology of intracranial berry aneurysms. J Neurosurg. 1989; 70:823–831. [PubMed: 2654334]
33. Steiger HJ, Aaslid R, Keller S, Reulen HJ. Strength, elasticity and viscoelastic properties of cerebral aneurysms. Heart Vessels. 1989; 5:41–46. [PubMed: 2584177]
34. Stemper BD, Yoganandan N, Stineman MR, Gennarelli TA, Baisden JL, Pintar FA. Mechanics of fresh, refrigerated, and frozen arterial tissue. J Surg Res. 2007; 139(2):236–242. [PubMed: 17303171]
35. The International Study of Unruptured Intracranial Aneurysms Investigators. Unruptured intracranial aneurysms-risk of rupture and risks of surgical intervention. N Engl J Med. 1998; 339(24):1725–1733. [PubMed: 9867550]
36. Weir, B.; Macdonald, RL. Intracranial aneurysms and subarachnoid hemorrhage: an overview. In: Wilkins, RH.; Rengachany, SS., editors. Neurosurgery. 2. New York: McGraw-Hill; 1996. p. 2191-2213.
37. Wiebers DO, Torner JC, Meissner I. Impact of unruptured intracranial aneurysms on public health in the united states. Stroke. 1992; 23:1416–1419. [PubMed: 1412577]

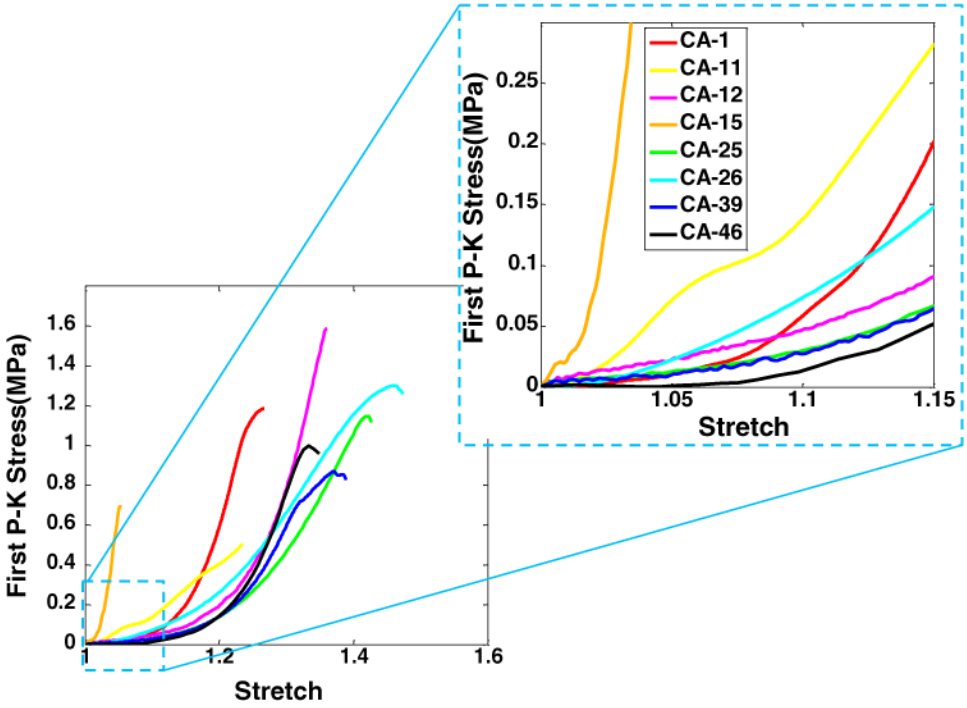

FIGURE 1.

Results for stress (1st Piola-Kirkoff) vs. stretch for the uniaxial loading tests to failure for eight aneurysm samples. A magnified insert is included to enlarge the low stress region.

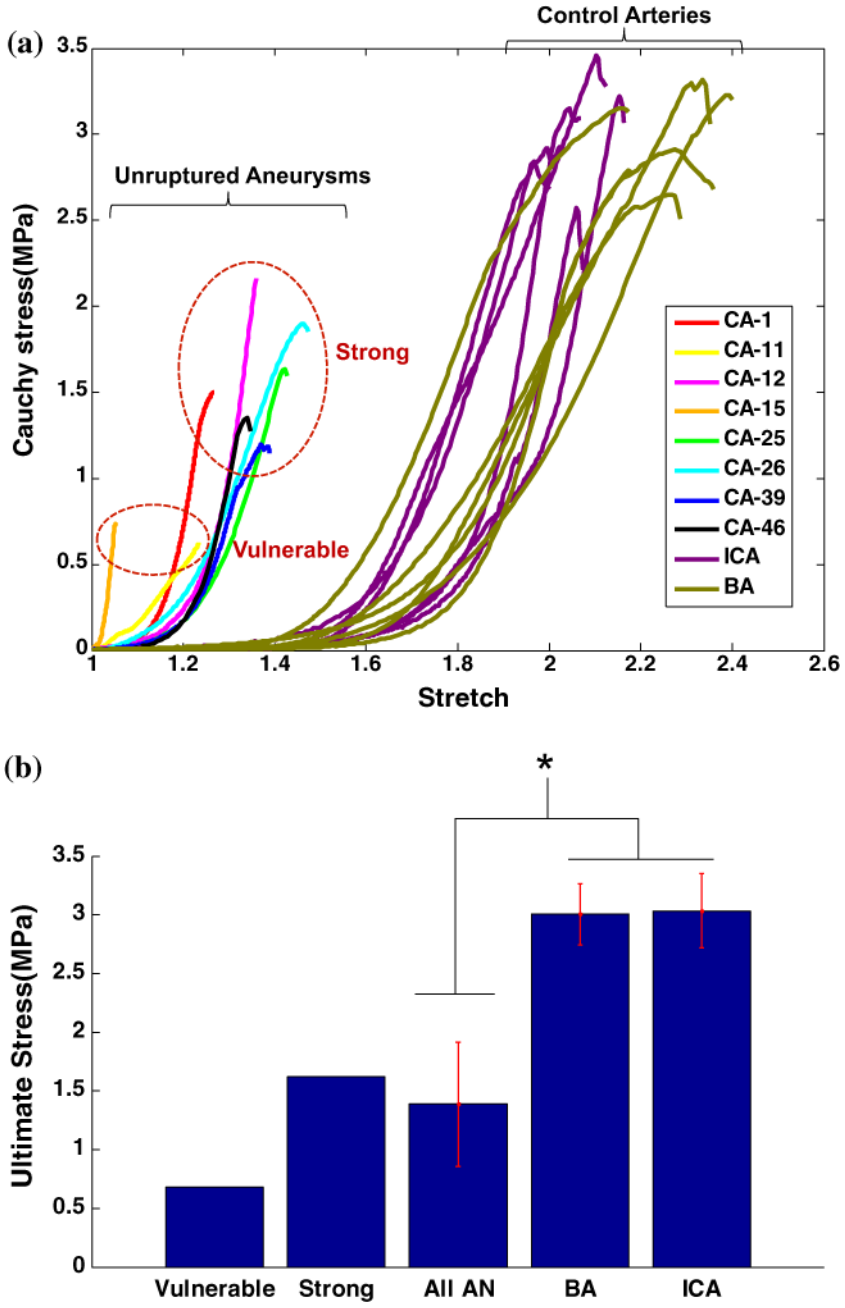

FIGURE 2.

Results for the uniaxial loading tests for eight human aneurysm samples (unruptured) and twelve human control (basilar and internal carotid) arteries. All tissues were tested to failure. In (a) the stress (Cauchy) vs. stretch is shown. The loading curves for the more vulnerable aneurysm samples are qualitatively different from the stronger samples. All aneurysm samples are weaker than the control arteries and displayed a greatly shortened toe region. In (b) the average failure stress (Cauchy) and standard deviation are shown for aneurysms and control arteries.

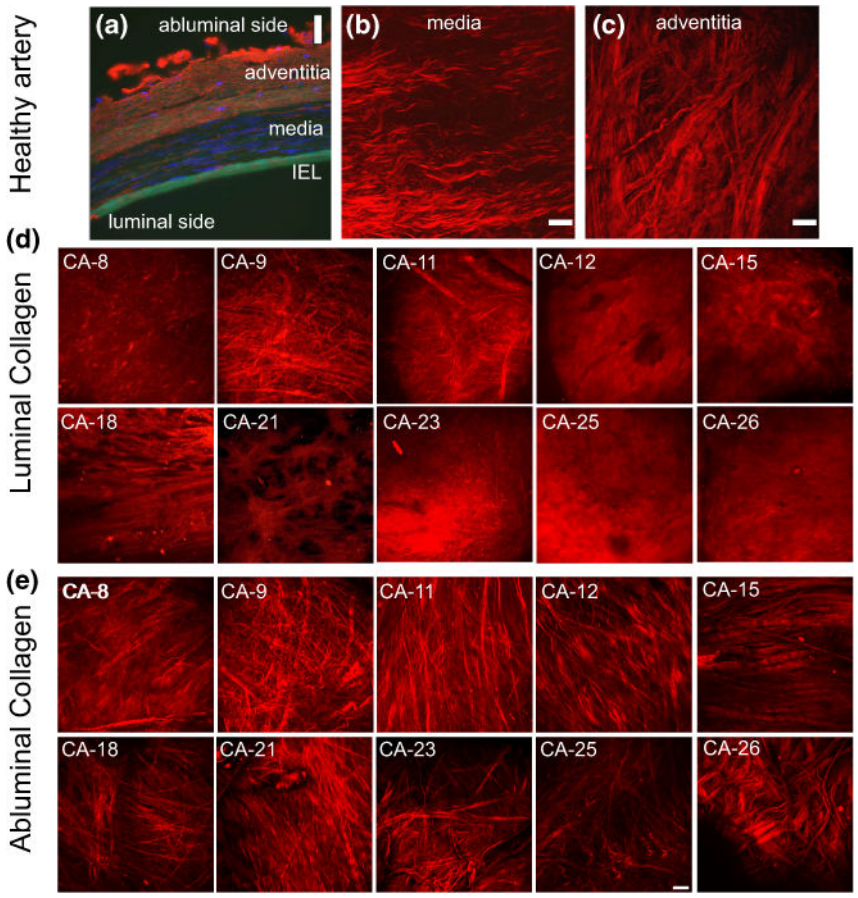

FIGURE 3.

Images of the aneurysm and basilar wall structure. In (a) fluorescence microscopy image of cross sectional preparation of the human left vertebral artery (cerebral) fixed at 30% stretch. The immunohistochemical staining of the arterial wall reveals elastin (green) localized in the internal elastic lamina, cell nuclei (blue, DAPI stain), type III collagen fibers (red). (b) and (c) display collagen fibers in projected stacks of multiphoton images of the media and adventitia, respectively, for a basilar control artery. Projected stacks of multiphoton images for collagen fibers seen in the luminal and abluminal sides of the aneurysm are shown in (d) and (e), respectively. Substantial variability in the collagen fiber architecture can be seen in the luminal images. Scale bars in all figures are 50 μm. ((a) is obtained from Robertson *et al.*[23] with permission from Springer).

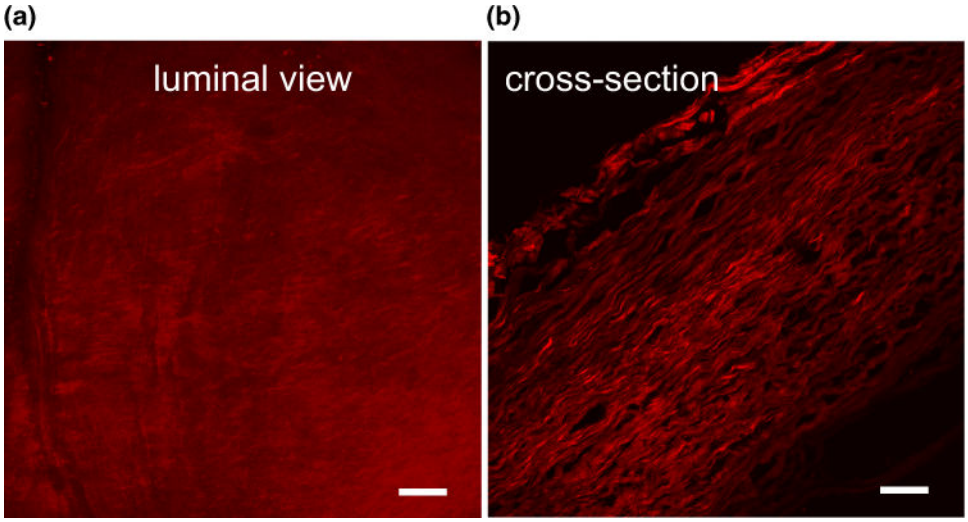

FIGURE 4.

Luminal view (a) from sample CA-26 displaying an abnormally dense collagen signal relative to that from the control artery. A cross sectional view of this sample (b), showing increased layering of collagen fibers and increased wall thickness relative to control arteries for example seen in Fig. 3a. Scale bars in all figures are 50 μm.

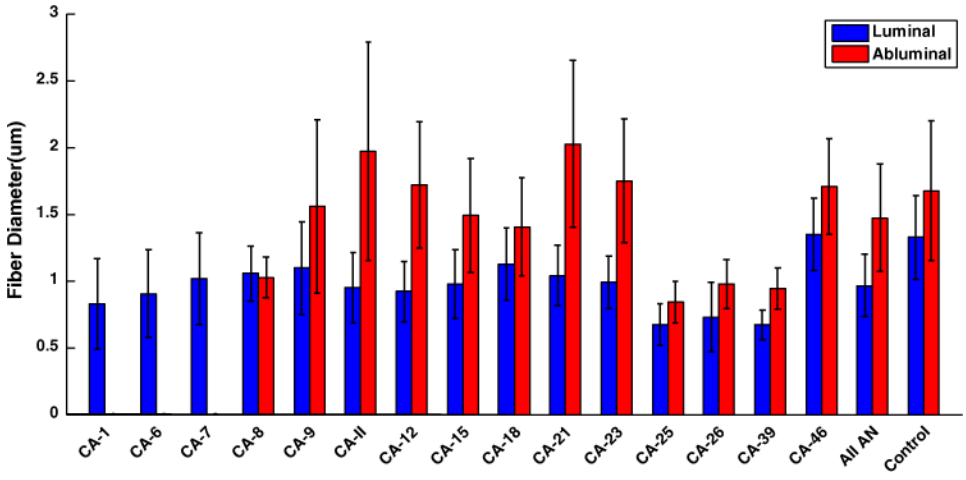

FIGURE 5.

Results for collagen fiber diameter obtained for projected stacks from cerebral aneurysm and cerebral artery tissue. The bars show average fiber diameter for a single location along with standard deviation.

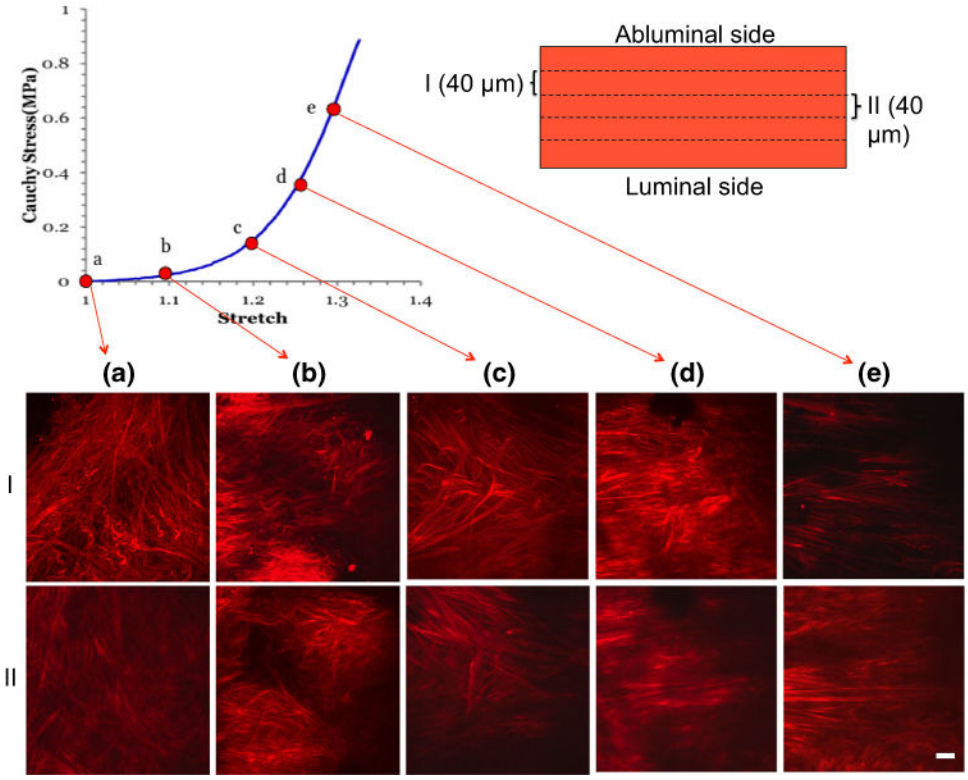

FIGURE 6.

Recruitment of collagen fibers during uniaxial loading of a single sample obtained using the UA-MPM system for CA-25 at stretches of (a) 1.0; (b) 1.1; (c) 1.2; (d) 1.26; (e) 1.3. Images are obtained from a projection of stacks over an approximately 40 μm width of tissue. The images in rows I and II are obtained at a depth of approximately 40 and 80 μm, respectively, relative to the abluminal surface. Scale bars 50 μm.

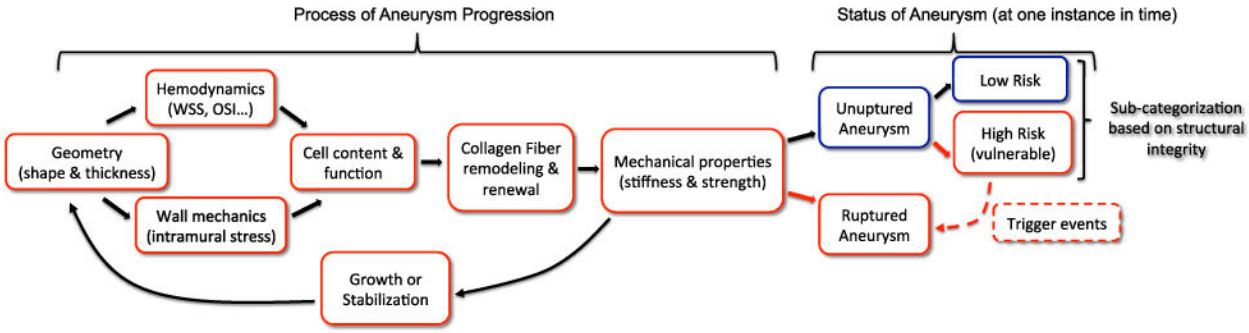

FIGURE 7.

Schematic of the coupled factors driving aneurysm progression toward stabilization or growth, illustrating how the mechanical loading drives cellular response which in turn drives the collagen production/turnover process (either pathological or normal), that in turn determines the mechanical properties of the wall. These properties then determine the geometry of the aneurysm wall under the given loads. At a given point in time, the status of the aneurysm is either ruptured or unruptured. Using a structural integrity index, the unruptured aneurysms can be categorized as low risk (strong) or high risk (vulnerable). The high risk aneurysms have the potential to shift to the ruptured category given an appropriate trigger event such as rise in blood pressure. When the subcategorization in unruptured status is available, correlations can be explored between wall structure and cell content and strong vs. vulnerable/ruptured walls.

TABLE 1

Summary of clinical data for the 15 aneurysm cases.

ID	Location resected IA	Age	Gender	Symptomatic?	SAH	Family history IA?	No. of IAs	Cigarette smoker? (Packs/week)	Hypertension?	Diabetic?
CA-1	MCA	61	F	Yes	No	Yes	1	Yes (10)	Yes	No
CA-6	MCA	62	F	Yes	No	No	1	No	No	No
CA-7	MCA	53	M	Yes	No	No	1	Yes (7)	Yes	No
CA-8	ICA	46	F	Yes	No	Yes	2	Yes (7)	No	No
CA-9	ICA	27	M	Incidental	No	Yes	1	–	No	No
CA-11	ICA	63	M	Incidental	No	No	2	No	Yes	Yes
CA-12	MCA	69	M	Incidental	No	Yes	3	No	No	No
CA-15	MCA	69	F	Incidental	No	No	2	Yes (1)	No	No
CA-18	ACA (distal)	56	F	Yes	No	No	4	Yes (7)	No	No
CA-21	ICA	57	M	Yes	No	No	3	Yes (10)	No	No
CA-23	MCA	54	M	Yes	No	No	3	No	No	No
CA-25	AcomA	53	F	Yes	No	Yes	2	No	No	No
CA-26	ACA (distal)	50	M	Yes	No	No	1	No	No	No
CA-39	MCA	61	F	Yes	No	No	4	No	Yes	No
CA-46	MCA	66	F	Incidental	No	No	1	Yes(7)	Yes	No

All aneurysms were unruptured.

MCA: middle cerebral artery; AcomA: anterior communicating artery; ICA: internal cerebral artery; ACA: anterior cerebral artery.

TABLE 2

Morphology of the aneurysm sac and dome wall.

	Lumen morphology								
ID	Volume (mm^3)	Surface area (mm^2)	Equiv. diam. (mm)	Max. an. size (mm)	An. depth (mm)	Neck area (mm^2)	Neck max. size (mm)	Aspect ratio	Wall morphology Wall thickness (mm)
CA-1	440	275	9.4	11.9	9.3	26.9	6.5	1.4	0.24
CA-6	90	100	5.6	8.1	5.6	20.3	5.2	1.1	0.13
CA-7	110	105	5.9	7.9	6.0	22.4	6.6	0.9	0.23
CA-8	710	405	11.1	16.2	14.9	20.0	5.1	3.0	0.19
CA-9	290	215	8.2	10.6	8.9	24.9	5.7	1.6	0.16
CA-11	215	170	7.5	9.2	7.1	18.3	4.9	1.4	0.21
CA-12	65	80	5.0	7.2	6.2	6.9	3.0	2.0	0.20
CA-15	420	270	9.3	11.6	9.4	36.0	7.0	1.3	0.13
CA-18	45	55	4.4	6.0	4.0	18.5	5.2	0.8	0.22
CA-21	110	110	5.9	7.5	6.3	16.4	4.7	1.3	0.20
CA-23	50	60	4.6	5.6	4.5	12.8	4.3	1.0	0.17
CA-25	45	60	4.4	5.8	4.1	12.3	4.3	0.9	0.24
CA-26	160	145	6.7	9.3	7.4	17.0	5.6	1.3	0.45
CA-39	170	160	6.9	10.3	6.8	22.6	5.7	1.2	0.21
CA-46	495	285	9.8	11.7	9.3	39.8	9.2	1.0	0.30

TABLE 3

Mechanical properties of aneurysm dome and control arteries.

ID	Trans. stretch	Low strain stiffness (MPa)	High strain stiffness (MPa)	Ultimate stretch	Ultimate stress (Cauchy) (MPa)	Ultimate stress (1st PK) (MPa)	Ultimate tension (kg/s^2)	$C0_1$ (MPa)	$C0_2$	R_2
Aneurysm domes										
CA-1	1.15	0.37	14.75	1.27	1.50	1.19	285	5.47	1.10	0.986
CA-11	1.10	1.72	3.42	1.24	0.625	0.51	105	3.76	0.54	0.872
CA-12	1.26	0.62	18.84	1.36	2.16	1.59	320	1.79	5.69	0.999
CA-15	1.02	2.10	25.06	1.05	0.73	0.70	90	338.13	0.54	0.962
CA-25	1.23	0.26	8.25	1.42	1.63	1.15	280	1.40	0.68	0.999
CA-26	1.21	0.95	7.37	1.47	1.90	1.30	580	1.84	0.54	0.981
CA-39	1.22	0.33	8.35	1.37	1.20	0.87	183	1.26	7.32	0.999
CA-46	1.23	0.24	12.99	1.33	1.34	1.00	300	1.45	8.38	0.994
Avg	1.18	0.82	12.38	1.31	1.39	1.04	268	44.39	3.10	
Basilar arteries										
BA-1	1.52	0.05	5.94	2.16	3.15	1.46	374	0.160	0.224	0.989
BA-2	1.68	0.05	5.36	2.31	3.30	1.43	365	0.096	0.036	0.974
BA-3	1.61	0.04	4.51	2.27	2.65	1.17	255	0.104	0.043	0.990
BA-4	1.77	0.17	7.15	2.27	2.91	1.28	390	0.062	0.174	0.999
BA-5	1.79	0.08	5.44	2.39	3.23	1.35	400	0.071	0.038	0.993
BA-6	1.81	0.05	8.88	2.17	2.79	1.29	430	0.063	0.121	0.951
Avg	1.70	0.08	6.21	2.26	3.01	1.33	369	0.093	0.106	
Internal carotid arteries										
ICA-1	1.81	0.06	5.95	2.04	3.15	1.54	400	0.029	0.498	0.996
ICA-2	1.60	0.03	7.10	2.03	2.93	1.45	363	0.071	0.566	0.982
ICA-3	1.64	0.05	3.02	2.15	3.22	1.50	525	0.042	0.209	0.994
ICA-4	1.82	0.07	10.03	2.06	2.58	1.25	413	0.031	0.353	0.996
ICA-5	1.66	0.12	8.68	1.97	2.84	1.45	421	0.110	0.241	0.993
ICA-6	1.56	0.07	6.03	2.10	3.48	1.66	415	0.185	0.101	0.982
Avg	1.68	0.07	6.80	2.06	3.03	1.47	423	0.08	0.33	

BA: basilar artery; ICA: internal carotid artery, adjacent to circle of Willis.